

Programmable Photonic Time Circuits for Highly Scalable Universal Unitaries

Xianji Piao¹, Sunkyu Yu^{2,*}, and Namkyoo Park^{3,†}

¹Wave Engineering Laboratory, School of Electrical and Computer Engineering, University of Seoul, Seoul 02504, Korea

²Intelligent Wave Systems Laboratory, Department of Electrical and Computer Engineering, Seoul National University, Seoul 08826, Korea

³Photonic Systems Laboratory, Department of Electrical and Computer Engineering, Seoul National University, Seoul 08826, Korea

 (Received 20 August 2023; accepted 1 February 2024; published 5 March 2024)

Programmable photonic circuits (PPCs) have garnered substantial interest for their potential in facilitating deep learning accelerations and universal quantum computations. Although photonic computation using PPCs offers ultrafast operation, energy-efficient matrix calculations, and room-temperature quantum states, its poor scalability hinders integration. This challenge arises from the temporally one-shot operation of propagating light in conventional PPCs, resulting in a light-speed increase in device footprints. Here we propose the concept of programmable photonic time circuits, utilizing time-cycle-based computations analogous to gate cycling in the von Neumann architecture and quantum computation. Our building block is a reconfigurable $SU(2)$ time gate, consisting of two resonators with tunable resonances, and coupled via time-coded dual-channel gauge fields. We demonstrate universal $U(N)$ operations with high fidelity using an assembly of the $SU(2)$ time gates, substantially improving scalability from $O(N^2)$ to $O(N)$ in terms of both the footprint and the number of gates. This result paves the way for PPC implementation in very large-scale integration.

DOI: [10.1103/PhysRevLett.132.103801](https://doi.org/10.1103/PhysRevLett.132.103801)

A programmable photonic circuit (PPC) is a versatile platform for neuromorphic and quantum computation [1,2], providing run-time tunability along with the advantages of photonics—ultrafast processing, robust quantum states [3,4], and energy-efficient matrix calculation [5–7]. PPCs particularly enable universal and reconfigurable unitary operations, $U(N)$, essential for trainable weight matrices in wave neural networks [5] and programmable quantum gates [8,9]. Conventional $U(N)$ PPCs comprise $SU(2)$ gates, implemented using beam splitters and phase shifters [2], and their arrangements and gate parameters are systematically determined [10,11].

In realizing large-scale wave neural networks [7] and qudit systems [4] with $U(N)$ PPCs, two major hurdles remain: fidelity and footprint. First, as PPC size increases, the demand for high-fidelity platforms becomes more crucial due to growing manufacturing errors and thermal noises. Consistent efforts have been made to improve PPC fidelity using self-calibration [12], optomechanics [13], and circuit pruning [14]. Another challenge, exacerbating the first hurdle, is poor scalability. This difficulty arises from the operation principle of PPCs: $U(N)$ operations of propagating light, leading to a light-speed increase of an optical path length. Consequently, the two-dimensional (2D) PPC footprint, which is proportional to the product of the optical path length and the channel number, exhibits $O(N^2)$ scaling for both the footprint and gate number in traditional algorithms [10,11].

Significant efforts have been conducted to resolve the scaling issue. Recent attempts to realize highly integrated PPCs using subwavelength optics [15] or diffractive elements [16–18] still maintain $O(N^2)$ scaling. An elegant approach that utilizes the frequency synthetic dimension [19] has enabled $O(N)$ scaling in PPC size, yet requiring N multiwavelength-coded light sources and detectors. Therefore, realizing high- N unitary PPCs with enhanced scalability through single wavelength operations still remains a significant challenge. Revisiting various computations that utilize the temporal axis—fetch-execute cycles [20], qubit-gate cycles [21], and synaptic plasticity [22]—we envision incorporating a temporal degree of freedom into PPCs.

Here we develop a PPC platform that achieves $O(N)$ scaling for reconfigurable, universal, and single-wavelength unitary operations. Inspired by space-time duality, which has introduced photonic time crystals [23,24], disorder [25,26], and diffraction [27], we propose programmable photonic “time” circuits (PPTCs) that replace optical path length with field evolution time. As a unit element, we devise an $SU(2)$ time gate, which enables universal $SU(2)$ operations on stored light. We demonstrate $U(N)$ PPTCs for random Haar matrices and quantum Fourier transforms (QFTs), achieving $O(N)$ scaling in both the footprint and gate number. This result offers a scalable platform for photonic deep learning accelerators and quantum computations.

Concept.—We compare the photonic realizations of a unitary matrix $U_N \in U(N)$ each employing conventional PPC [Fig. 1(a)] and our PPTC [Fig. 1(b)]. The building blocks of both circuits are SU(2) gates, which utilize propagating modes [Fig. 1(c)] and resonance modes [Fig. 1(d)], respectively. In realizing U_N with SU(2) gates, conventional approaches involve a nulling process [10,11] [Fig. 1(e)]. This process sets all the off-diagonal elements of U_N to zero by sequentially multiplying the matrices T to U_N , where $T \in U(N)$ performs the SU(2) gate operation on two specific channels while preserving the others. Consequently, realizing U_N requires $N(N-1)/2$ SU(2) gates, which corresponds to the number of pairs of sub- and super-diagonal elements.

Among the algorithms for designing $U(N)$ PPCs [10,11], the Clements design [11] offers more integrated and loss-tolerant PPCs than the original Reck design [10], by adopting a symmetric gate arrangement that enables the

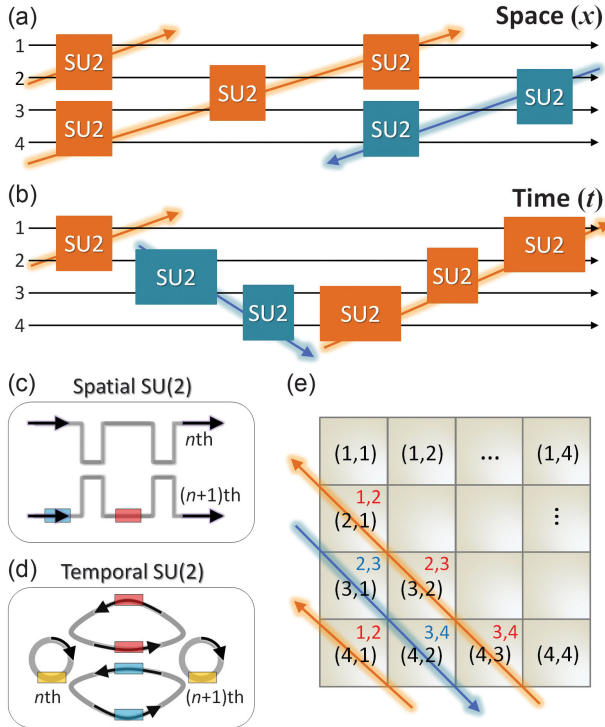


FIG. 1. PPTCs with $O(N)$ scalability. (a),(b), $U(4)$ PPC (a) and $U(4)$ PPTC (b). “SU2” boxes indicate the SU(2) operations with their lengths indicating the spatial or temporal footprint. (c),(d) SU(2) gates between the n th and $(n+1)$ th channels in the PPC (c) and PPTC (d): Mach-Zehnder interferometers (gray lines), phase shifters (colored boxes), resonators (circles), and nonresonant waveguide loops (curved triangles). Phase shifters are applied to resonators (yellow boxes) and waveguides (red and blue boxes). Black arrows in (a)–(d) denote wave evolutions. (e) Nulling process. The pairs (p, q) (black) denote wave evolutions. r, s (red or blue) represent the matrix element index and the SU(2)-coupling channels for nulling the (p, q) element, respectively. Colored arrows in (a),(b) depict the nulling processes, corresponding to the arrows in (e).

simultaneous execution of $(N-1)/2$ SU(2) operations on average [Fig. 1(a)]. However, regardless of whether the Reck or Clements design is employed, the resulting PPCs exhibit the same $O(N^2)$ scaling in both their footprints and gate numbers (Table S1 in [28]). This poor scalability is incompatible with large-scale deep learning and noisy intermediate-scale quantum computing (NISQ). For instance, considering a conventional SU(2) gate with a footprint of approximately 0.5 mm^2 [13], a unitary matrix for 1000 photonic neurons or 10 qubits would require a footprint of about 0.5 m^2 and approximately 10^6 pairs of passive and active elements.

To tackle this hurdle, we propose the PPTC, which utilizes the *time* evolution coordinate [47–49]. We assign the resonance mode of each resonator to a channel, enabling $O(N)$ scaling in the footprint by replacing optical path length [Fig. 1(a)] with evolution time [Fig. 1(b)]. Because SU(2) operations are performed with stored light, the unit SU(2) gate must be reconfigurable, which facilitates $O(N)$ scaling in the gate number (Table S1 in [28]).

SU(2) time gates.—A key challenge in replacing spatial propagation with temporal evolution in resonators lies in developing a temporal analog of reconfigurable and universal SU(2) space gates. Considering the SU(2) space gate composed of Mach-Zehnder interferometers and phase shifters [Fig. 1(c)], the SU(2) time gate requires time-varying coupling and resonances. However, achieving such a temporal equivalent with reconfigurability presents a significant challenge because coupling is primarily determined by the fixed spatial distance between resonators.

To address this challenge, we develop the SU(2) time gate as the fundamental building block of the PPTC, which takes the form of a resonator lattice. At the operating frequency, each resonator of the PPTC supports the pseudospin modes of clockwise ($\sigma = +1$) and counterclockwise ($\sigma = -1$) wave circulations [50]. Adjacent resonators are coupled via two nonresonant, single-mode waveguide loops [50,51] [Fig. 2(a)]. The coupling strength between resonators is then determined by the decay rate $1/\tau$ of both pseudo-spin modes to a waveguide loop. For the upper (“U”) and lower (“L”) paths of the loop between the m th and n th resonators, we apply the time-varying phase differences to drive dynamical dual-channel gauge fields $\xi_{mn}^U(t)$ and $\xi_{mn}^L(t)$, each having opposite signs for pseudospin modes. The tight-binding Hamiltonian of the resonator lattice is (note S1 in [28])

$$H = - \sum_{m,\sigma} [\omega_0 + \Delta\omega_m(t)] a_{m\sigma}^\dagger a_{m\sigma} - \frac{1}{2\tau} \sum_{(m,n),\sigma} [(e^{-i\sigma\xi_{mn}^U(t)} + e^{-i\sigma\xi_{mn}^L(t)}) a_{m\sigma}^\dagger a_{n\sigma} + \text{H.c.}], \quad (1)$$

where ω_0 is the reference resonance frequency, $\Delta\omega_m(t)$ is the resonance perturbation of the m th resonator, $a_{m\sigma}^\dagger$ and

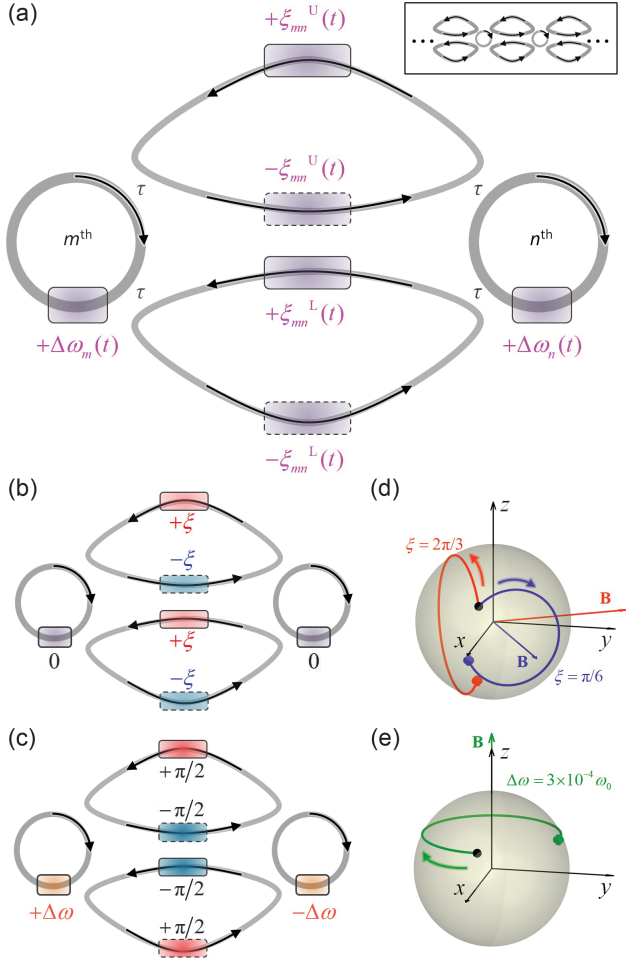


FIG. 2. SU(2) time gate. (a) Schematic diagram: circles for resonators and curved triangles for waveguide loops. Shaded boxes represent phase shifters. The inset represents the PPTC composed of time gates. (b),(c) System states with the even-parity (b) and odd-parity (c) gauges. Black arrows in (a)–(c) indicate wave circulations. (d),(e) Spinor evolutions for the even-parity states (d) with $\xi = 2\pi/3$ (red) and $\xi = \pi/6$ (blue), and the odd-parity state (e) with $\Delta\omega = 3 \times 10^{-4}\omega_0$. Black dots denote initial states. $0 \leq t \leq 0.8\pi\tau$. Supplemental Material movies 1–3 show the evolutions in (b) and (c).

$a_{m\sigma}$ are the creation and annihilation operators for the σ pseudo-spin at the m th site, respectively, $\langle m, n \rangle$ is the neighboring site indices, and H.c. denotes the Hermitian conjugate. The unit cell of the lattice—two coupled resonators—in Fig. 2(a) operates as the SU(2) time gate.

Given that U_N is realized with a set of SU(2) operations [10,11], we investigate a range of operations accessible with a SU(2) time gate, setting $\xi_{mn}^{U,L}(t) = \xi^{U,L}(t)$, $\Delta\omega_m(t) = +\Delta\omega(t)$, and $\Delta\omega_n(t) = -\Delta\omega(t)$. For the $\sigma = +1$ mode of which the field amplitude in the p th resonator is ψ_p , we introduce the spinor $\Psi = [\psi_m, \psi_n]^T$ satisfying $id\Psi/dt = H_S\Psi$, where the Hamiltonian H_S is (note S2 in [28])

$$H_S = -\omega_0\sigma_0 - \frac{1}{2\tau} [\cos \xi^U(t) + \cos \xi^L(t)]\sigma_x - \frac{1}{2\tau} [\sin \xi^U(t) + \sin \xi^L(t)]\sigma_y - \Delta\omega(t)\sigma_z, \quad (2)$$

and σ_0 and $\sigma_{x,y,z}$ are the identity matrix and Pauli matrices, respectively.

Because of the time-varying system parameters, Eqs. (1) and (2) lead to nonlinear dynamics. To gain clearer insight, we impose the linearized picture by assuming the digital modulation: setting the constant gauge fields and resonance perturbation as $\xi^{U,L}(t) = \xi^{U,L}$ and $\Delta\omega(t) = \Delta\omega$ during a specific temporal range. For the Stokes vector [52] $\mathbf{S} = [S_x, S_y, S_z]^T$ where $S_j = \Psi^\dagger \sigma_j \Psi$ ($j = x, y$, and z), the geometrical evolution of \mathbf{S} on the Bloch sphere is governed by $d\mathbf{S}/dt = \mathbf{S} \times \mathbf{B}$, where the pseudomagnetic field \mathbf{B} is (note S3 in [28])

$$\mathbf{B} = \frac{2}{\tau} \left[\frac{\cos \xi^U + \cos \xi^L}{2}, \frac{\sin \xi^U + \sin \xi^L}{2}, \Delta\omega\tau \right]^T. \quad (3)$$

Equation (3) demonstrates that the spinor evolution in the SU(2) time gate is analogous to the Larmor precession [53]. The evolution also corresponds to the SU(2) rotation of the spinor Ψ (note S4 in [28]) for the spinor Hamiltonian $H_S = -\omega_0\sigma_0 - \mathbf{B} \cdot \boldsymbol{\sigma}/2$, where $\boldsymbol{\sigma} = \mathbf{e}_x\sigma_x + \mathbf{e}_y\sigma_y + \mathbf{e}_z\sigma_z$ is the Pauli vector.

According to Eq. (3), we define two fundamental system states (Note S5 in [28]): even-parity gauges without resonance perturbations [Fig. 2(b); $\xi^U = \xi^L = \xi$ and $\Delta\omega = 0$], and odd-parity gauges with resonance perturbations [Fig. 2(c); $\xi^U = -\xi^L = \pi/2$ and $\Delta\omega \neq 0$]. The even and odd states correspond to the spinor rotations about \mathbf{B} on the xy plane [Fig. 2(d)] and along the z axis [Fig. 2(e)], respectively, allowing seamless coverage of the Bloch sphere by controlling time t .

U(N) operations.—By employing the conventional nulling process outlined in the Clements design [11], we develop the combination of SU(2) time gates for U(N) PPTCs (note S6 in [28]). This nulling process under the linearized picture derives the time-coded digital modulation of system parameters applied to the universal unitary operations of PPTCs. We note that the designed U(N) PPTCs perform computations through gate cycling instead of the one-shot, spatial computations found in conventional PPCs, by reconfiguring SU(2) time gates dynamically.

Considering the upper limit of modulation speed for refractive index changes, determined by various index modulation mechanisms—such as all-optical [54,55], electro-optical [56–58], or thermo-optical [59] schemes—we assume the first-order low-pass filtering (LPF) for time-coded modulation signals (note S7 in [28]). For LPF modulations with the cutoff frequency ω_c , we conduct the time-domain analysis using the sixth-order Runge-Kutta (RK6) method [60] (note S7 in [28]). Although

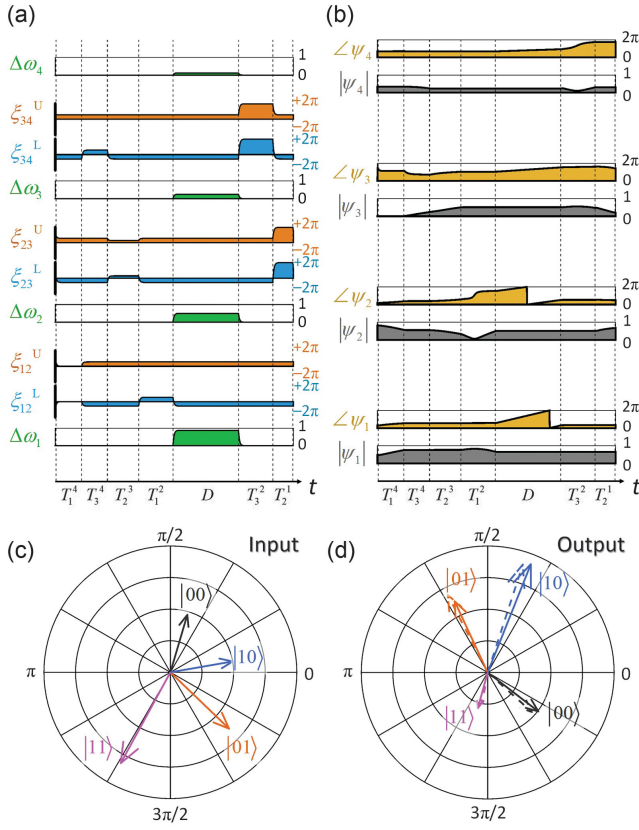


FIG. 3. QFT PPTC. (a) Time-coded modulations of $\Delta\omega_q$ and $\xi_{(p,p+1)}^{U,L}$ for the two-qubit QFT ($1 \leq p \leq 3, 1 \leq q \leq 4$). The signals undergo LPF with $\omega_c = \omega_0/100$, where ω_0 is the operating frequency. (b) The corresponding temporal evolutions of the state vectors ψ_q . The temporal cells T_m^l and D are the unitary and diagonal matrices, which are the decomposition matrices of U^{QFT} (note S6 in [28] for details). (c),(d) An example of the input (c) and QFT output (d). Resonance fields representing qubit states $|00\rangle, |01\rangle, |10\rangle$, and $|11\rangle$ are depicted in the complex plane. In (d), the solid and dashed lines describe the PPTC output and ideal solution, respectively. $\tau = 500 \times (2\pi/\omega_0)$.

we obtain the modulation signals under the linearization, we apply the RK6 method to the nonlinear Eq. (1) directly to demonstrate the validity of our assumption.

As the first example, we examine the unitary matrix $U^{\text{QFT}} \in U(N)$ for the two-qubit QFT [61] ($N = 2^2$) achieved with the PPTC. Using the time-coded modulations obtained through the LPF [Fig. 3(a)], the amplitude and phase of the field inside each resonator are tailored [Fig. 3(b)]. Figures 3(c) and 3(d) show an example of the input and output of the two-qubit QFT. As shown in Fig. 3(d), the output (solid lines) aligns closely with the expected solution (dashed lines). A slight deviation, likely due to the LPF, necessitates a more in-depth quantitative analysis, which we will address subsequently.

Fidelity and measurement.—We investigate the fidelity of the PPTC for the QFT, and more generally, universal unitaries: sampling the $U(N)$ group uniformly with the

Haar measure [62] to generate K realizations of random Haar matrices $U_k^{\text{Haar}} \in U(N)$ ($k = 1, 2, \dots, K$). When we realize unitary matrices using the PPTC, the time-coded modulations result in nonunitary operations because Eq. (1) is nonlinear. Therefore, we develop a stochastic model to evaluate the PPTC fidelity (note S7 in [28]). The model utilizes L effective matrix operations $\{V^{\text{QFT},l}\}$ for U^{QFT} and $\{V_k^{\text{Haar},l}\}$ for U_k^{Haar} ($l = 1, 2, \dots, L$) obtained from the relationship between M random inputs and their corresponding outputs calculated by the RK6 method, where $L, M \gg N$. By employing the fidelity [14] comparing the effective $N \times N$ matrix V to U

$$F(U, V) = \frac{2\text{Re}[\text{Tr}(V^\dagger U)]}{N + \text{Tr}(V^\dagger V)}, \quad (4)$$

the fidelities are obtained as $F^{\text{QFT}} \equiv \langle F(U^{\text{QFT}}, V^{\text{QFT},l}) \rangle_l$ and $F_k^{\text{Haar}} \equiv \langle F(U_k^{\text{Haar}}, V_k^{\text{Haar},l}) \rangle_l$, where $\langle \dots \rangle_l$ represents the ensemble average across realizations denoted by index l .

We calculate the fidelities F^{QFT} and F_k^{Haar} for different LPF bandwidths [Fig. 4(a)], comparing $N = 4$ and $N = 8$ in realizing Haar and QFT matrices. The result shows that higher ω_c leads to better fidelities owing to the better conservation of the designed modulation signals. Although the importance of ω_c becomes more significant as N increases, three-qubit ($N = 8$) PPTCs achieve $F^{\text{Haar}} \geq 0.95$ for $\omega_c \geq 0.006\omega_0$, where $F^{\text{Haar}} \equiv \langle F_k^{\text{Haar}} \rangle_k$ is the averaged fidelity with U_k^{Haar} . The decrease in fidelity originates from our digital modulation scheme with LPF [Fig. 3(a)]. Techniques in digital signal processing [63], such as predistortion, can be employed to compensate for this fidelity degradation. In note S8 of [28], we present an example of predistortion employing inverse filtering, which demonstrates a substantial enhancement in fidelities ($F^{\text{Haar}} > 0.80$ across the entire range of $\omega_c \geq 0.001\omega_0$).

Figure 4(b) illustrates a measurement setup employing probe waveguides, similar to conventional approaches [50,51] (note S7 in [28] for numerical analysis). The waveguides are coupled to each resonator with an identical lifetime τ_e , while ensuring distinct optical paths for the incident (φ_n^+) and scattering waves (φ_n^-). When we excite a temporally bounded pulse and normalize the scattering power $\sum_n |\varphi_n^-|^2$, the probe waveguides with an identical τ_e do not impact the fidelity (note S9 in [28]). However, as shown in Fig. 4(c), the ratio τ_e/τ determines the scattering power. When $\tau_e \gg \tau$ (lower inset), the probe waveguide is coupled too weakly to the PPTC to effectively excite inputs. In contrast, when $\tau_e \ll \tau$ (upper inset), the excited fields decay too rapidly during the operations. Therefore, the competition between the excitation and decay results in an N -dependent optimum point in τ_e/τ .

To assess the potential performance of PPTCs in practical implementations, we examine the effect of nonuniform system parameters on fidelity, including variations in

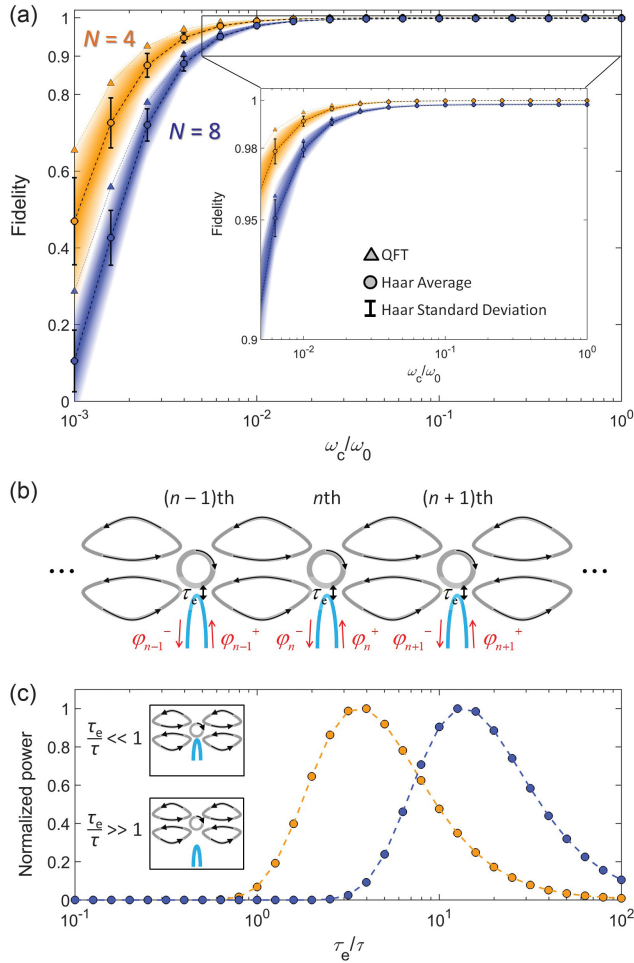


FIG. 4. Fidelity and measurement. (a) PPTC fidelities as functions of ω_c in the LPF: F^{QFT} (triangles) and F^{Haar} (circles) with $N = 4$ (orange, 2 qubits) and $N = 8$ (blue, 3 qubits). The inset in (a) presents the range of the fidelity larger than 0.9. Circles and error bars show the average and standard deviation of $K = 20$ random realizations at each ω_c , respectively. $M = 100$ and $L = 100$. (b) Schematic diagram of the measurement setup, coupling probe waveguides (blue) to resonators. Red arrows denote the incident (φ_n^+) and scattering (φ_n^-) waves. (c) Scattering power for $N = 4$ (orange, 2 qubits) and $N = 8$ (blue, 3 qubits) PPTCs as a function of τ_e to each probe waveguide. $\omega_c = \omega_0$ in (c). For each τ_e , we apply 100 normalized random incidences with the Dirac-delta-function-like excitations into the PPTC. All the other parameters are the same as those in Fig. 3 and note S7 in [28].

resonant frequencies, intrinsic loss, and external coupling (note S10 in [28]). The result indicates that achieving the uniformity of the systems would be critical for realizing high-fidelity PPTCs, while a fidelity of approximately ≥ 0.95 for $N = 4$ is achievable with conventional technology in integrated photonics. Further discussion on scalability and future research is provided in note S11 of [28].

In conclusion, we proposed a reconfigurable and universal $U(N)$ platform, using temporal degrees of freedom in line with recent efforts on the space-time analogy,

such as photonic time crystals [23,24] and disorder [26]. The systematic design of time-coded modulations for high-fidelity unitaries was demonstrated. We envisage the simultaneous utilization of space-time degrees of freedom for programmable photonics, considering recent studies [64,65].

We acknowledge financial support from the National Research Foundation of Korea (NRF) through the Basic Research Laboratory (No. 2021R1A4A3032027), Young Researcher Program (No. 2021R1C1C1005031), and Mid-career Researcher Program (No. RS-2023-00274348), all funded by the Korean government. This work was supported by Creative-Pioneering Researchers Program and the BK21 FOUR program of the Education and Research Program for Future ICT Pioneers in 2023, through Seoul National University. We also acknowledge an administrative support from SOFT foundry institute.

*sunkyu.yu@snu.ac.kr

†nkpark@snu.ac.kr

- [1] N. C. Harris, J. Carolan, D. Bunandar, M. Prabhu, M. Hochberg, T. Baehr-Jones, M. L. Fanto, A. M. Smith, C. C. Tison, and P. M. Alsing, Linear programmable nanophotonic processors, *Optica* **5**, 1623 (2018).
- [2] W. Bogaerts, D. Pérez, J. Capmany, D. A. Miller, J. Poon, D. Englund, F. Morichetti, and A. Melloni, Programmable photonic circuits, *Nature (London)* **586**, 207 (2020).
- [3] S. Takeda and A. Furusawa, Toward large-scale fault-tolerant universal photonic quantum computing, *APL Photonics* **4**, 060902 (2019).
- [4] Y. Chi, J. Huang, Z. Zhang, J. Mao, Z. Zhou, X. Chen, C. Zhai, J. Bao, T. Dai, and H. Yuan, A programmable qudit-based quantum processor, *Nat. Commun.* **13**, 1166 (2022).
- [5] Y. Shen, N. C. Harris, S. Skirlo, M. Prabhu, T. Baehr-Jones, M. Hochberg, X. Sun, S. Zhao, H. Larochelle, D. Englund, and M. Soljačić, Deep learning with coherent nanophotonic circuits, *Nat. Photonics* **11**, 441 (2017).
- [6] H. Zhou, J. Dong, J. Cheng, W. Dong, C. Huang, Y. Shen, Q. Zhang, M. Gu, C. Qian, and H. Chen, Photonic matrix multiplication lights up photonic accelerator and beyond, *Light Sci. Appl.* **11**, 30 (2022).
- [7] S. Pai, Z. Sun, T. W. Hughes, T. Park, B. Bartlett, I. A. Williamson, M. Minkov, M. Milanizadeh, N. Abebe, and F. Morichetti, Experimentally realized *in situ* backpropagation for deep learning in photonic neural networks, *Science* **380**, 398 (2023).
- [8] J. Wang, F. Sciarrino, A. Laing, and M. G. Thompson, Integrated photonic quantum technologies, *Nat. Photonics* **14**, 273 (2020).
- [9] J. Carolan, C. Harrold, C. Sparrow, E. Martín-López, N. J. Russell, J. W. Silverstone, P. J. Shadbolt, N. Matsuda, M. Oguma, and M. Itoh, Universal linear optics, *Science* **349**, 711 (2015).

- [10] M. Reck, A. Zeilinger, H. J. Bernstein, and P. Bertani, Experimental realization of any discrete unitary operator, *Phys. Rev. Lett.* **73**, 58 (1994).
- [11] W. R. Clements, P. C. Humphreys, B. J. Metcalf, W. S. Kolthammer, and I. A. Walmsley, Optimal design for universal multiport interferometers, *Optica* **3**, 1460 (2016).
- [12] X. Xu, G. Ren, T. Feleppa, X. Liu, A. Boes, A. Mitchell, and A. J. Lowery, Self-calibrating programmable photonic integrated circuits, *Nat. Photonics* **16**, 595 (2022).
- [13] M. Dong, G. Clark, A. J. Leenheer, M. Zimmermann, D. Dominguez, A. J. Menssen, D. Heim, G. Gilbert, D. Englund, and M. Eichenfield, High-speed programmable photonic circuits in a cryogenically compatible, visible–near-infrared 200 mm CMOS architecture, *Nat. Photonics* **16**, 59 (2022).
- [14] S. Yu and N. Park, Heavy tails and pruning in programmable photonic circuits for universal unitaries, *Nat. Commun.* **14**, 1853 (2023).
- [15] P. Cheben, R. Halir, J. H. Schmid, H. A. Atwater, and D. R. Smith, Subwavelength integrated photonics, *Nature (London)* **560**, 565 (2018).
- [16] T. Zhou, X. Lin, J. Wu, Y. Chen, H. Xie, Y. Li, J. Fan, H. Wu, L. Fang, and Q. Dai, Large-scale neuromorphic optoelectronic computing with a reconfigurable diffractive processing unit, *Nat. Photonics* **15**, 367 (2021).
- [17] H. Zhu, J. Zou, H. Zhang, Y. Shi, S. Luo, N. Wang, H. Cai, L. Wan, B. Wang, and X. Jiang, Space-efficient optical computing with an integrated chip diffractive neural network, *Nat. Commun.* **13**, 1044 (2022).
- [18] T. Fu, Y. Zang, Y. Huang, Z. Du, H. Huang, C. Hu, M. Chen, S. Yang, and H. Chen, Photonic machine learning with on-chip diffractive optics, *Nat. Commun.* **14**, 70 (2023).
- [19] S. Buddhiraju, A. Dutt, M. Minkov, I. A. Williamson, and S. Fan, Arbitrary linear transformations for photons in the frequency synthetic dimension, *Nat. Commun.* **12**, 2401 (2021).
- [20] J. L. Hennessy and D. A. Patterson, *Computer Architecture: A Quantitative Approach* (Elsevier, New York, 2011).
- [21] F. Arute, K. Arya, R. Babbush, D. Bacon, J. C. Bardin, R. Barends, R. Biswas, S. Boixo, F. G. Brandao, and D. A. Buell, Quantum supremacy using a programmable superconducting processor, *Nature (London)* **574**, 505 (2019).
- [22] A. Holtmaat and K. Svoboda, Experience-dependent structural synaptic plasticity in the mammalian brain, *Nat. Rev. Neurosci.* **10**, 647 (2009).
- [23] E. Lustig, Y. Sharabi, and M. Segev, Topological aspects of photonic time crystals, *Optica* **5**, 1390 (2018).
- [24] M. Lyubarov, Y. Lumer, A. Dikopoltsev, E. Lustig, Y. Sharabi, and M. Segev, Amplified emission and lasing in photonic time crystals, *Science* **377**, 425 (2022).
- [25] Y. Sharabi, E. Lustig, and M. Segev, Disordered photonic time crystals, *Phys. Rev. Lett.* **126**, 163902 (2021).
- [26] J. Kim, D. Lee, S. Yu, and N. Park, Unidirectional scattering with spatial homogeneity using correlated photonic time disorder, *Nat. Phys.* **19**, 726 (2023).
- [27] R. Tirole, S. Vezzoli, E. Galiffi, I. Robertson, D. Maurice, B. Tilmann, S. A. Maier, J. B. Pendry, and R. Sapienza, Double-slit time diffraction at optical frequencies, *Nat. Phys.* **19**, 999 (2023).
- [28] See Supplemental Material at <http://link.aps.org/supplemental/10.1103/PhysRevLett.132.103801> for (Table S1) scalabilities of PPCs and PPTCs, (note S1) tight-binding Hamiltonian for coupled resonator lattices, (note S2) the spinor Hamiltonian for an SU(2) time gate, (note S3) Larmor precession of a spinor, (note S4) universal rotations with SU(2) gates, (note S5) rotation operators of parity states, (note S6) nulling process for universal unitaries, (note S7) time-domain analysis, (note S8) precompensation of refractive index modulations, (note S9) fidelity in the presence of uniformly distributed loss, (note S10) fidelity in the presence of disorder, and (note S11) practical implementation, which includes Refs. [29–46].
- [29] C. Manolatos, M. Khan, S. Fan, P. R. Villeneuve, H. Haus, and J. Joannopoulos, Coupling of modes analysis of resonant channel add-drop filters, *IEEE J. Quantum Electron.* **35**, 1322 (1999).
- [30] H. Kuratsuji and S. Kakigi, Maxwell-Schrödinger equation for polarized light and evolution of the Stokes parameters, *Phys. Rev. Lett.* **80**, 1888 (1998).
- [31] S. Yu, X. Piao, and N. Park, Acceleration toward polarization singularity inspired by relativistic $E \times B$ drift, *Sci. Rep.* **6**, 37754 (2016).
- [32] S. Yu, X. Piao, and N. Park, Designing non-Hermitian dynamics for conservative state evolution on the Bloch sphere, *Phys. Rev. A* **97**, 033805 (2018).
- [33] Q. Xu, B. Schmidt, S. Pradhan, and M. Lipson, Micrometre-scale silicon electro-optic modulator, *Nature (London)* **435**, 325 (2005).
- [34] J. D. Joannopoulos, S. G. Johnson, J. N. Winn, and R. D. Meade, *Photonic Crystals: Molding the Flow of Light* (Princeton University Press, Princeton, NJ, 2011).
- [35] Y. Qu, M. Zhou, E. Khoram, N. Yu, and Z. Yu, Resonance for analog recurrent neural network, *ACS Photonics* **9**, 1647 (2022).
- [36] H. Lee, T. Chen, J. Li, K. Y. Yang, S. Jeon, O. Painter, and K. J. Vahala, Chemically etched ultrahigh-Q wedge-resonator on a silicon chip, *Nat. Photonics* **6**, 369 (2012).
- [37] S. Yu, C.-W. Qiu, Y. Chong, S. Torquato, and N. Park, Engineered disorder in photonics, *Nat. Rev. Mater.* **6**, 226 (2021).
- [38] B. Ouyang, Y. Xing, W. Bogaerts, and J. Caro, Silicon ring resonators with a free spectral range robust to fabrication variations, *Opt. Express* **27**, 38698 (2019).
- [39] H. Jung, C. Xiong, K. Y. Fong, X. Zhang, and H. X. Tang, Optical frequency comb generation from aluminum nitride microring resonator, *Opt. Lett.* **38**, 2810 (2013).
- [40] M. W. Puckett, K. Liu, N. Chauhan, Q. Zhao, N. Jin, H. Cheng, J. Wu, R. O. Behunin, P. T. Rakich, and K. D. Nelson, 422 Million intrinsic quality factor planar integrated all-waveguide resonator with sub-MHz linewidth, *Nat. Commun.* **12**, 934 (2021).
- [41] M. Hafezi, S. Mittal, J. Fan, A. Migdall, and J. Taylor, Imaging topological edge states in silicon photonics, *Nat. Photonics* **7**, 1001 (2013).
- [42] A. J. Kollár, M. Fitzpatrick, and A. A. Houck, Hyperbolic lattices in circuit quantum electrodynamics, *Nature (London)* **571**, 45 (2019).

- [43] Y. Wang, Z. Hu, B. C. Sanders, and S. Kais, Qudits and high-dimensional quantum computing, *Front. Phys.* **8**, 589504 (2020).
- [44] Z. Zhou, X. Ou, Y. Fang, E. Alkhazraji, R. Xu, Y. Wan, and J. E. Bowers, Prospects and applications of on-chip lasers, *Elight* **3**, 1 (2023).
- [45] S. Gyger, J. Zichi, L. Schweickert, A. W. Elshaari, S. Steinhauer, S. F. Covre da Silva, A. Rastelli, V. Zwiller, K. D. Jöns, and C. Errando-Herranz, Reconfigurable photonics with on-chip single-photon detectors, *Nat. Commun.* **12**, 1408 (2021).
- [46] H. Zhang, M. Gu, X. Jiang, J. Thompson, H. Cai, S. Paesani, R. Santagati, A. Laing, Y. Zhang, and M. Yung, An optical neural chip for implementing complex-valued neural network, *Nat. Commun.* **12**, 457 (2021).
- [47] W. Krolikowski, O. Bang, J. J. Rasmussen, and J. Wyller, Modulational instability in nonlocal nonlinear Kerr media, *Phys. Rev. E* **64**, 016612 (2001).
- [48] E. Turitsyna, S. Smirnov, S. Sugavanam, N. Tarasov, X. Shu, S. Babin, E. Podivilov, D. Churkin, G. Falkovich, and S. Turitsyn, The laminar–turbulent transition in a fibre laser, *Nat. Photonics* **7**, 783 (2013).
- [49] D. Churkin, S. Sugavanam, N. Tarasov, S. Khorev, S. Smirnov, S. Kobtsev, and S. Turitsyn, Stochasticity, periodicity and localized light structures in partially mode-locked fibre lasers, *Nat. Commun.* **6**, 7004 (2015).
- [50] M. Hafezi, E. A. Demler, M. D. Lukin, and J. M. Taylor, Robust optical delay lines with topological protection, *Nat. Phys.* **7**, 907 (2011).
- [51] S. Yu, X. Piao, and N. Park, Topological hyperbolic lattices, *Phys. Rev. Lett.* **125**, 053901 (2020).
- [52] M. C. Teich and B. Saleh, *Fundamentals of Photonics* (Wiley Interscience, New York, 2007).
- [53] D. J. Griffiths, *Introduction to Quantum Mechanics* (Prentice-Hall, Englewood Cliffs, NJ, 1995).
- [54] V. R. Almeida, C. A. Barrios, R. R. Panepucci, and M. Lipson, All-optical control of light on a silicon chip, *Nature (London)* **431**, 1081 (2004).
- [55] M. Ono, M. Hata, M. Tsunekawa, K. Nozaki, H. Sumikura, H. Chiba, and M. Notomi, Ultrafast and energy-efficient all-optical switching with graphene-loaded deep-subwavelength plasmonic waveguides, *Nat. Photonics* **14**, 37 (2020).
- [56] S. Y. Siew, B. Li, F. Gao, H. Y. Zheng, W. Zhang, P. Guo, S. W. Xie, A. Song, B. Dong, and L. W. Luo, Review of silicon photonics technology and platform development, *J. Lightwave Technol.* **39**, 4374 (2021).
- [57] C. T. Phare, Y.-H. Daniel Lee, J. Cardenas, and M. Lipson, Graphene electro-optic modulator with 30 GHz bandwidth, *Nat. Photonics* **9**, 511 (2015).
- [58] K. Powell, L. Li, A. Shams-Ansari, J. Wang, D. Meng, N. Sinclair, J. Deng, M. Lončar, and X. Yi, Integrated silicon carbide electro-optic modulator, *Nat. Commun.* **13**, 1851 (2022).
- [59] Z. Fang, R. Chen, J. Zheng, A. I. Khan, K. M. Neilson, S. J. Geiger, D. M. Callahan, M. G. Moebius, A. Saxena, and M. E. Chen, Ultra-low-energy programmable non-volatile silicon photonics based on phase-change materials with graphene heaters, *Nat. Nanotechnol.* **17**, 842 (2022).
- [60] J. C. Butcher, On Runge-Kutta processes of high order, *J. Aust. Math. Soc.* **4**, 179 (1964).
- [61] M. A. Nielsen and I. Chuang, *Quantum Computation and Quantum Information* (Cambridge Univ. Press, Cambridge, 2011).
- [62] A. Haar, Der Massbegriff in der Theorie der kontinuierlichen Gruppen, *Ann. Math.* **34**, 147 (1933).
- [63] J. G. Proakis and D. K. Manolakis, *Digital Signal Processing: Principles, Algorithms, and Applications, 4/E* (Prentice-Hall, London, 2006).
- [64] J. Park and B. Min, Spatiotemporal plane wave expansion method for arbitrary space–time periodic photonic media, *Opt. Lett.* **46**, 484 (2021).
- [65] J. Park, H. Cho, S. Lee, K. Lee, K. Lee, H. C. Park, J.-W. Ryu, N. Park, S. Jeon, and B. Min, Revealing non-Hermitian band structure of photonic Floquet media, *Sci. Adv.* **8**, eabo6220 (2022).